HHS Public Access

Author manuscript

Med Phys. Author manuscript; available in PMC 2025 January 01.

Published in final edited form as:

Med Phys. 2024 January ; 51(1): 522–532. doi:10.1002/mp.16729.

Technical note: Impact of Dose Voxel Kernel (DVK) values on dosimetry estimates in ^{177}Lu and ^{90}Y Radiopharmaceutical Therapy (RPT) applications

Rachele Danieli[1,2,3], **Daniele Pistone**[4,5,6,*], **Jonathan Tranel**[7], **Francesca Botta**[8], **Carlos Uribe-Munoz**[9,10], **Davide Raspanti**[11], **Francesc Salvat**[12], **Scott J Wilderman**[13], **Manuel Bardiès**[14,15], **Ernesto Amato**[4,5,16], **Yuni K Dewaraja**[17], **Marta Cremonesi**[18]

[1]Université libre de Bruxelles (ULB), Hôpital Universitaire de Bruxelles (H.U.B), Institut Jules Bordet, Department of Medical Physics, Brussels, Belgium

[2]Université Libre De Bruxelles (ULB), Radiophysics and MRI Physics Laboratory, Brussels, Belgium

[3]Université libre de Bruxelles (ULB), Hôpital Universitaire de Bruxelles (H.U.B), Institut Jules Bordet, Department of Nuclear Medicine, Brussels, Belgium

[4]Department of Biomedical and Dental Sciences and of Morphologic and Functional Imaging (BIOMORF), University of Messina, Messina, Italy

[5]National Institute for Nuclear Physics (INFN), section of Catania, Catania, Italy

[6]Università degli Studi della Campania “Luigi Vanvitelli”, Dipartimento di Matematica e Fisica, Caserta, Italy

[7]Department of Radiology and Biomedical Imaging, University of California San Francisco, San Francisco, CA 94143, USA

[8]Medical Physics Unit, Instituto Europeo di Oncologia IRCCS, via Ripamonti 435, 20141 Milan, Italy

[9]Department of Radiology, University of British Columbia, Vancouver, British Columbia, Canada

[10]Functional Imaging, BC Cancer, Vancouver, British Columbia, Canada

[11]Temasinergie S.p.A., Via Marcello Malpighi 120, 48018 Faenza, Italy

[12]Facultat de Física (FQA and ICC), Universitat de Barcelona, Diagonal 645, 08028 Barcelona, Catalonia, Spain

[13]Department of Nuclear Engineering and Radiological Sciences, University of Michigan, Ann Arbor, Michigan

[14]Département de Médecine Nucléaire, Institut Régional du Cancer de Montpellier (ICM), Montpellier F-34298, France

[*]**Correspondence:** Daniele Pistone, Dipartimento di Matematica e Fisica, Università degli Studi della Campania “Luigi Vanvitelli”, Viale Lincoln 5, 81100 Caserta, Italy. daniele.pistone@unicampania.it.

Conflict of Interest

Yuni Dewaraja is a consultant for MIM Software.

[15]IRCM, UMR 1194 INSERM, Université de Montpellier and Institut Régional du Cancer de Montpellier (ICM), Montpellier F-34298, France

[16]Health Physics Unit, University Hospital “Gaetano Martino”, Messina, Italy

[17]Department of Radiology, University of Michigan, Ann Arbor, Michigan

[18]Radiation Research Unit, Instituto Europeo di Oncologia IRCCS, Via Giuseppe Ripamonti 435, 20141 Milano, Italy

Abstract

Background: Radiopharmaceutical Therapy (RPT) is an increasingly adopted modality for treating cancer. There is evidence that the optimization of the treatment based on dosimetry can improve outcomes. However, standardization of the clinical dosimetry workflow still represents a major effort. Among the many sources of variability, the impact of using different Dose Voxel Kernels (DVKs) to generate absorbed dose (AD) maps by convolution with the time-integrated activity (TIA) distribution has not been systematically investigated.

Purpose: This study aims to compare DVKs and assess the differences in the ADs when convolving the same TIA map with different DVKs.

Methods: DVKs of 3×3×3 mm^3 sampling - nine for ^{177}Lu, nine for ^{90}Y - were selected from those most used in commercial/free software or presented in prior publications. For each voxel within a 11×11×11 matrix, the coefficient of variation (CoV) and the percentage difference between maximum and minimum values (% maximum difference) were calculated. The total absorbed dose per decay (SUM), calculated as the sum of all the voxel values in each kernel, was also compared. Publicly available quantitative SPECT images for two patients treated with ^{177}Lu-DOTATATE and PET images for two patients treated with ^{90}Y-microspheres were used, including organs at risk (^{177}Lu: kidneys; ^{90}Y: liver and healthy liver) and tumors’ segmentations. For each patient, the mean AD to the volumes of interest (VOIs) was calculated using the different DVKs, the same TIA map and the same software tool for dose convolution, thereby focusing on the DVK impact. For each VOI, the % maximum difference of the mean AD between maximum and minimum values was computed.

Results: The CoV (% maximum difference) in voxels of normalized coordinates [0,0,0], [0,1,0] and [0,1,1] were 5%(21%), 9%(35%) and 10%(46%) for the ^{177}Lu DVKs. For the case of ^{90}Y, these values were 2%(9%), 4%(14%) and 4%(16%). The CoV (% maximum difference) for SUM was 9%(33%) for ^{177}Lu, and 4%(15%) for ^{90}Y. The variability of the mean tumor and organ AD was up to 19% and 15% in ^{177}Lu-DOTATATE and ^{90}Y-microspheres patients, respectively.

Conclusions: This study showed a considerable AD variability due exclusively to the use of different DVKs. A concerted effort by the scientific community would contribute to decrease these discrepancies, strengthening the consistency of AD calculation in RPT.

Keywords

Dose-Voxel-Kernel; ^{90}Y; ^{177}Lu; patient-specific dosimetry; radionuclide therapy

Introduction and background

In Radiopharmaceutical Therapy (RPT), three-dimensional (3D) voxel-level internal dosimetry is receiving increasing attention, driven by the interest in estimating not only the average absorbed dose (AD) to volumes of interest (VOIs), but also the AD non-uniformity due to the non-uniform spatial distribution of activity. The starting point for 3D voxel-level dosimetry is 3D voxel-level activity maps, derived from quantitative tomographic images (i.e. PET or SPECT scans) acquired at single or multiple time-points. Following voxel-level time-integration techniques, a time-integrated activity (TIA) map can be computed and, by means of one of the approaches described below, converted into a 3D AD map[1].

To date, three different approaches are available for AD map calculation[2]:

- **i.** Local Energy Deposition (LED), which assumes the energy released in a voxel of the TIA map to be absorbed within the same voxel. LED typically includes the contribution of charged particles and ignores the one of photons;
- **ii.** Convolution of a Dose Voxel Kernel (DVK) with a TIA map, where a DVK is defined as a 3D voxel matrix representing the mean AD to a target voxel per decay event in the central source voxel, both of which are contained in an infinite homogeneous medium. DVKs are sometimes referred to also as Voxel S-factors (VSFs) or Voxel S-Values (VSVs);
- **iii.** Direct Monte Carlo (MC) simulation of the radionuclide decays that uses the distribution from a TIA map and tracks all the transport and interactions between the emitted radiation and the patient's body where different materials are modeled from CT imaging.

Direct MC radiation transport is considered, at least in principle, the most accurate and personalized approach for internal dosimetry as it takes into account the heterogeneity of the tissue density and composition. Because MC simulations require relevant computational resources and expertise, however, LED and convolution algorithms are more frequently adopted for clinical dosimetry[3].

DVKs are generally calculated exploiting MC simulations[4]. However, different MC codes and different processes - e.g. direct MC simulation, MC-based volume integration of a dose-point kernel (DPK), which is the radial distribution of the AD per decay event due to an isotropic point source located inside a virtually infinite and homogeneous absorbing medium, and MC-derived analytical methods - have been adopted by different authors to generate the actual DVKs from simulations. Even if some sets of DVKs have been compared to each other[5], to our knowledge no specific investigation of the impact of using different DVKs on the AD calculation has been carried out yet in a systematic manner.

The aim of this work is to assess the differences in the ADs when convolving the same TIA map with different DVKs. This has been done using a set of 18 commonly adopted or recently developed DVKs for ^{177}Lu and ^{90}Y and using imaging data from patients treated with ^{177}Lu-DOTATATE and with ^{90}Y-microspheres.

Materials and methods

Dose voxel kernels

We used a total of 18 different DVKs with details given in Tables 1 (for ^{177}Lu) and 2 (for ^{90}Y). For ^{177}Lu, nine DVKs with voxel sizes of 3×3×3mm^3 and matrix sizes ranging from 11×11×11 to 275×275×275 were compared. Among them, five were generated by direct MC simulation (Lanconelli[6], Pistone[7], Salvat, Tranel and UMICH DPM), two were derived from DPKs (Graves[8] and Vergara[9]), and two were computed based on analytical methods (Amato[10] and Pistone_AM[7]). For ^{90}Y, nine DVKs with voxel sizes of 3×3×3 mm^3 and matrix sizes from 11×11×11 to 17×17×17 were selected. Six of the selected ^{90}Y DVKs were computed by direct MC simulation (Bolch[11], Lanconelli[6], Pistone, Salvat, Tranel and UMICH DPM), two starting from a DPK (Graves[8] and Vergara[9]) and one with an analytical method (Amato[10]). Note that because ^{90}Y is a pure beta emitter (i.e. there are no gamma emissions) and given that the range of its beta particles in tissue (maximum range in soft tissue: 11 mm) is much shorter than gammas, the kernel matrix size of ^{90}Y that accounts for a complete energy deposition of the emitted particles is smaller than for ^{177}Lu.

Comparison of DVKs

For each voxel in a 11×11×11 matrix, the coefficient of variation (CoV) – defined as the standard deviation divided by the mean - and the percentage difference between the maximum and the minimum values across all the selected DVKs normalized by the minimum (% maximum difference) were computed. In addition, normalized DVKs were generated by dividing each DVK value by the average value obtained with all the DVKs. The total absorbed dose per decay (SUM), calculated as the sum of all the voxel values in each kernel, was also compared. Given a DVK with matrix size N×N×N, SUM was computed as:

$$SUM = [0,0,0] + \sum_{i=i}^{N} 2 * [i,0,0] + \sum_{j=1}^{N} 2 * [0,j,0] + \sum_{k=1}^{N} 2 * [0,0,k] + \sum_{i=1}^{N} \sum_{j=1}^{N} 4 * [i,j,0] + \sum_{i=1}^{N} \sum_{k=1}^{N} 4 * [i,0,k] + \sum_{j=1}^{N} \sum_{k=1}^{N} 4 * [0,j,k] + \sum_{i=1}^{N} \sum_{j=1}^{N} \sum_{k=1}^{N} 8 * [i,j,k]$$

All the DVKs used in the study are available in the Supplemental Material.

Comparison of ADs on Patient Data

Quantitative post-therapy ^{177}Lu SPECT/CT images of two patients treated with ^{177}Lu-DOTATATE[12] and ^{90}Y PET/CT images of two patients treated with ^{90}Y-microspheres[13] were used. These data are publicly available in the University of Michigan Deep Blue Data Repository.[12,14] The ^{177}Lu-DOTATATE data is the same used in the Society of Nuclear Medicine ^{177}Lu Dosimetry Challenge.[14,15] Segmentations of organs at risk (OARs) - kidneys[16] for the two ^{177}Lu-DOTATATE patients, and whole and normal liver for the two ^{90}Y-microspheres patients – and tumors were also provided [14,15]. For each patient, the AD maps were calculated using the different DVKs coupled with the same dosimetry software, MIM SurePlan MRT (MIM Software, USA), thereby focusing on the impact

specifically of the DVK. Before performing the dosimetry, all the selected DVKs were manually imported into the software. For ^{177}Lu, SPECT images acquired at four different time-points were registered and segmentations were propagated from the reference time-point (24 h) to the others. Next, ^{177}Lu time-activity curves generated for each VOI were fitted to a sum of exponentials defined according to the Akaike Information Criterion. After the time-integration at the VOI level, ^{177}Lu TIA maps – one for each patient - were derived from the reference activity map by scaling the activity in each voxel by the ratio between the TIA computed at the VOI level to the total activity in the VOI corresponding to the voxel considered. For ^{90}Y, instead, a time-integration at the voxel-level considering only the physical decay was performed, as is standard because the microspheres do not redistribute. The resulting SPECT or PET-derived TIA maps, resampled to cubic voxel of 3 mm size, were converted into AD maps by means of a Fast Fourier Transform convolution with each of the selected DVKs. Finally, the AD maps were divided by a CT-based density map – also resampled to the DVK resolution – and manually multiplied by the mass density of the medium in which the DVKs were calculated to account for the difference between the latter and the actual tissue density. Excluding this last step, there was no manual intervention in the steps leading to the calculation of AD. For OARs and tumors, mean AD, D10 and D90 (i.e. the minimum AD to 10% and 90% of the volume, respectively) were computed. The average of the mean AD, D10 and D90 obtained with all the DVKs were calculated as well as the CoV and the % maximum difference. To further illustrate the variability among different DVKs, normalized mean AD were generated by dividing each mean AD by the average from all ADs.

Results

Comparison of DVKs

Figure 1 and 2 (top panels) show the selected ^{177}Lu and ^{90}Y DVKs as a function of the distance from the source voxel (intended as the distance from the geometric center of the source voxel, here and in the following), respectively. For ^{177}Lu, the source voxel of the DVK contributes to almost all its energy deposition, the maximum beta particle range in tissue being 2 mm. For ^{90}Y, in comparison, the contribution at voxels away from the source is more significant, due to the higher beta particle energy corresponding to a maximum range in tissue of 11 mm. Figure 1 and 2 (bottom panels) show the normalized DVKs as function of the distance from the source voxel. The CoV and the % maximum difference are plotted in Supplemental Fig S1.

For ^{177}Lu, CoV (% maximum difference) in voxels of normalized coordinates [0,0,0] (central voxel), [0,0,1] (3 mm from the center) and [0,1,1] (4.2 mm from the center) - which are the voxels giving the maximum contribution to the AD - were 5% (21%), 9% (35%), 10% (46%), respectively. For SUM, results were 9% (33%). Maximum differences were attributable to Lanconelli/Vergara (source voxel), Amato/UMICH DPM (voxels [0,0,1] and [0,1,1]) and Lanconelli/UMICH DPM (SUM). For ^{90}Y, CoV (% maximum difference) results were 2% (9%), 4% (14%) and 4% (16%) at voxels of coordinates [0,0,0], [0,0,1] and [0,1,1], respectively; 4% (15%) in SUM. In this case, Amato/Graves provides the maximum

difference in the source voxel, Lanconelli/Amato in the two diagonal voxels and Lanconelli/Vergara in SUM.

Comparison of ADs on Patient Data

For each patient, mean AD, D10 and D90 obtained with each selected DVK are provided in the Supplemental Tables S1–4. Average, CoV and % maximum difference of mean AD, D10 and D90 to kidneys (^{177}Lu), liver/healthy liver (^{90}Y) and tumors (^{177}Lu and ^{90}Y) are given in Table 3. Normalized mean AD are shown in Figure 3. For each VOI, maximum differences were attributable to Lanconelli/Vergara for both ^{177}Lu and ^{90}Y patients.

Discussion

There is increasing evidence that personalized dosimetry could play an important role in the optimization of RPT treatments[29]. Multicenter trials are therefore essential to explore AD-effect relationships allowing for that optimization[30]. The clinical dosimetry workflow, however, consists of different tasks, each of which can be performed in multiple ways. This lack of standardization prevents drawing conclusions from multicenter trials because of the discrepancies that might occur in the data among centers. The standardization of the clinical dosimetry workflow following RPT, therefore, still represents a major challenge for physicists in the field[15].

Many commercial and in-house software packages are now available for the computation of the AD and comparisons among them have been performed[31]. Such comparisons, however, usually do not allow a characterization of the variability associated to a single task within the clinical dosimetry workflow, for example the variability associated with the use of different algorithms for image registration or with the method for integrating the time-activity curve. Each software, in fact, offers different and limited solutions to perform the various tasks. The identification of the major sources of variability to be reduced in view of a standardization requires each of them to be isolated and analyzed separately from all the others. In this context, we aim to study the variability introduced when using different DVKs for the computation of the AD via convolution, while being fully aware that this may not be among the major sources of variability affecting the AD.

Our comparison showed that differences in the AD due only to the use of different DVKs are not negligible, with maximum values at the VOI level of 19% and 15% in patients treated with ^{177}Lu-DOTATATE and ^{90}Y-microspheres, respectively. These maximum differences were associated to the same pair of DVKs (Lanconelli/Vergara), perhaps indicating that these DVKs might be less accurate than other DVKs included in this comparison. Observed discrepancies were similar in different patients and VOIs (Figure 3).

Several factors, presented in Table 1, can contribute to the observed differences among the considered DVKs: the calculation method (e.g. direct MC simulation vs MC-based volume integration of DPKs), the nuclear data (e.g. RADAR spectra vs ICRP Publication 107), the definition of material density and composition (e.g. water vs soft tissue) or the MC code (e.g. Geant4 vs Penelope) and simulation parameters, such as the number of primaries, the energy/range cut-off and the physical models. Differences in the kernel size should be also

considered. The analysis of these factors and of their impact on the accuracy of DVKs is beyond the scope of this note, as our study was designed to assess variability and not accuracy.

A limitation of this study is that DVKs for only two different radioisotopes (^{177}Lu and ^{90}Y) were included. The inclusion of radionuclides with higher gamma emission probability and energy, e.g. 131I, would have been of interest to investigate the impact of different DVKs on the AD far from the source. Moreover, for each of the included radioisotopes, we considered patients treated with the same type of RPT (peptide receptor radionuclide therapy and radioembolization for ^{177}Lu and ^{90}Y, respectively), which means similar activity distributions. Finally, the results presented in this study are valid for a specific voxel size (3mm). When different voxel sizes are considered, higher or lower differences in the AD calculation can be in principle observed. Based on some limited comparisons already made, however, we can state that for voxel sizes other than 3 mm (range 2–4 mm) differences in the DVKs and mean ADs are generally of the same magnitude as those reported in this study. Exceptionally, however, AD differences up to 50% were found when including ^{177}Lu Graves' DVKs for sizes other than 3 mm, although we are aware that recently corrections have been made after the conclusion of our study [https://zenodo.org/record/7596345#.ZBLouHaZOUk]. We therefore recommend always benchmarking the DVK chosen for each specific voxel size, even for already published datasets. As example, the few investigated DVKs for sizes other than 3 mm (2.4 mm and 4 mm) are plotted in Supplemental Fig S2–3.

The RPT dosimetry community should be made aware of the magnitude of the differences in DVKs and the associated variability in patient AD estimates. Since the use of different DVKs is only one of the many possible sources of variability affecting the AD calculation, in fact, the final variability could be considerable and potentially impair the possibility to identify dose-effect relationships from multicenter data. Additional investigations are ongoing to assess the robustness of the various methods for DVK computation and to generate a standardized set of DVKs for the AD calculation.

Conclusions

This study shows substantial differences between DVKs from different sources that propagate into not negligible variability (up to 19%) in patient-specific AD due exclusively to the use of different DVKs. Among the many sources of variability affecting the calculation of the AD, the variability introduced by using different DVKs can be easily reduced by standardization, strengthening the consistency of AD calculation in RPT.

Supplementary Material

Refer to Web version on PubMed Central for supplementary material.

Acknowledgements

The authors acknowledge David Mirando for reviewing some comparisons. Yuni Dewaraja acknowledges grant support from R01CA240706 and R01EB022075 awarded by the National Institute of Health, USA. This work was partially supported by the Italian Ministry of Health with Ricerca Corrente and 5×1000 funds.

References

1. Sgouros G, Hobbs RF. Dosimetry for radiopharmaceutical therapy. Semin Nucl Med 2014;44(3):172–178. doi:10.1053/j.semnuclmed.2014.03.007 [PubMed: 24832581]
2. Bardies M, Vergara Gil A. ABSORBED DOSE CALCULATION. In: International Atomic Energy Agency (IAEA), ed. Dosimetry for Radiopharmaceutical Therapy [IAEA Preprint] Vienna (Austria); 2022:154–175. http://inis.iaea.org/search/search.aspx?orig_q=RN:53037189.
3. Della Gala G, Bardiès M, Tipping J, Strigari L. Overview of commercial treatment planning systems for targeted radionuclide therapy. Phys medica PM an Int J devoted to Appl Phys to Med Biol Off J Ital Assoc Biomed Phys 2021;92:52–61. doi:10.1016/j.ejmp.2021.11.001
4. Auditore L, Pistone D, Amato E, Italiano A. Monte Carlo methods in nuclear medicine. In: Signore A, ed. Nuclear Medicine and Molecular Imaging Elsevier; 2022:587–606. doi:10.1016/B978-0-12-822960-6.00136-8
5. Pacilio M, Lanconelli N, Lo MS, et al. Differences among Monte Carlo codes in the calculations of voxel S values for radionuclide targeted therapy and analysis of their impact on absorbed dose evaluations. Med Phys 2009;36(5):1543–1552. doi:10.1118/1.3103401 [PubMed: 19544770]
6. Lanconelli N, Pacilio M, Meo S Lo, et al. A free database of radionuclide voxel S values for the dosimetry of nonuniform activity distributions. Phys Med Biol 2012;57(2):517–533. doi:10.1088/0031-9155/57/2/517 [PubMed: 22217735]
7. Pistone D, Auditore L, Italiano A, Baldari S, Amato E. An analytic model to calculate Voxel S-Values for ^{177}Lu. Published online 2022. doi:10.1088/2057-1976/ac997e
8. Graves S, Tiwari A, Merrick M, et al. Accurate resampling of radial dose point kernels to a Cartesian matrix for voxelwise dose calculation Published online December 2020. doi:10.5281/ZENODO.3827983 (Version 1.1 at https://zenodo.org/record/7596345#.ZD1DPnbP2KJ)
9. Vergara Gil A OpenDoseDVKData https://gitlab.com/opendose/opendosedvkdata. Accessed September 9, 2022.
10. Amato E, Minutoli F, Pacilio M, Campennì A, Baldari S. An analytical method for computing voxel S values for electrons and photons. Med Phys 2012;39:6808–6817. doi:10.1118/1.4757912 [PubMed: 23127074]
11. Bolch WE, Bouchet LG, Robertson JS, et al. MIRD pamphlet no. 17: The dosimetry of nonuniform activity distributions - Radionuclide S values at the voxel level. J Nucl Med 1999;40(1).
12. Dewaraja YK, Van BJ. Lu-177 DOTATATE Anonymized Patient Datasets: Multi-Time Point Lu-177 SPECT/CT Scans. Univ Michigan - Deep Blue Data Published online 2021. doi:10.7302/0n8e-rz46
13. Van BJ, Dewaraja YK. Y-90 PET/CT & SPECT/CT and Corresponding Contours Dataset 31JULY2020. Univ Michigan - Deep Blue Data Published online 2020. doi:10.7302/pf4m-vn04
14. Uribe C, Peterson A, Van B, et al. An International Study of Factors Affecting Variability of Dosimetry Calculations, Part 1: Design and Early Results of the SNMMI Dosimetry Challenge. J Nucl Med 2021;62(Supplement 3):36S–47S. doi:10.2967/jnumed.121.262748 [PubMed: 34857620]
15. Uribe C, Brosch-Lenz J, Peterson A, et al. Variability in Dosimetry Calculations: an Analysis of the Results Submitted to the SNMMI Lu-177 Dosimetry Challenge. J Nucl Med 2022;63(supplement 2):2351.
16. Dewaraja YK, Van BJ. Lu-177 DOTATATE Anonymized Patient Datasets: Lesion and Organ Volumes of Interest. Univ Michigan - Deep Blue Data Published online 2021. doi:10.7302/vhrh-qg23
17. RAdiation Dose Assessment Resource (RADAR) - The Decay Data http://www.doseinfo-radar.com/RADARDecay.html. Accessed September 9, 2022.
18. National Nuclear Data Center. http://www.nndc.bnl.gov/index.jsp. Accessed March 1, 2018.
19. NUCLEIDE. http://www.nucleide.org/DDEP_WG/DDEPdata.htm. Accessed October 12, 2022.
20. García-Toraño E, Peyres V, Bé MM, Dulieu C, Lépy MC, Salvat F. Simulation of decay processes and radiation transport times in radioactivity measurements. Nucl Instruments Methods Phys Res Sect B Beam Interact with Mater Atoms 2017;396:43–49. doi:10.1016/j.nimb.2017.02.002

21. Agency NE. PENELOPE 2018: A Code System for Monte Carlo Simulation of Electron and Photon Transport; 2019. doi:10.1787/32da5043-en
22. Evaluated Nuclear Structure Data File https://www.nndc.bnl.gov/ensdf/. Accessed October 12, 2022.
23. National Nuclear Data Center NuDat (Nuclear Structure and Decay Data). NuDat 3.
24. Mougeot X Reliability of usual assumptions in the calculation of β and ν spectra. Phys Rev C 2015;91(5):55504. doi:10.1103/PhysRevC.91.055504
25. Van B, Dewaraja YK, Niedbala JT, et al. Experimental validation of Monte Carlo dosimetry for therapeutic beta emitters with radiochromic film in a 3D-printed phantom. Med Phys Published online August 2022. doi:10.1002/mp.15926
26. Cross WG. Variation of beta dose attenuation in different media. Phys Med Biol 1968;13(4):611–618. doi:10.1088/0031-9155/13/4/310 [PubMed: 5683329]
27. Eckerman KF, Westfall RJ, Ryman JC, Cristy M. Availability of nuclear decay data in electronic form, including beta spectra not previously published. Health Phys 1994;67(4):338–345. doi:10.1097/00004032-199410000-00004 [PubMed: 8083046]
28. Eckerman KF, Westfall RJ, Ryman JC, Cristy M. Nuclear Decay Data Files of the Dosimetry Research Group United States; 1993. http://inis.iaea.org/search/search.aspx?orig_q=RN:25039816.
29. Garin E, Tselikas L, Guiu B, et al. Personalised versus standard dosimetry approach of selective internal radiation therapy in patients with locally advanced hepatocellular carcinoma (DOSISPHERE-01): a randomised , multicentre , open-label phase 2 trial. Lancet Gastroenterol Hepatol 2020;1253(20):1–13. doi:10.1016/S2468-1253(20)30290-9
30. Taprogge J, Wadsley J, Miles E, Flux GD. Recommendations for Multicentre Clinical Trials Involving Dosimetry for Molecular Radiotherapy. Clin Oncol (R Coll Radiol) 2021;33(2):131–136. doi:10.1016/j.clon.2020.12.002 [PubMed: 33342617]
31. Mora-Ramirez E, Santoro L, Cassol E, et al. Comparison of commercial dosimetric software platforms in patients treated with ^{177}Lu-DOTATATE for peptide receptor radionuclide therapy. Med Phys 2020;47(9):4602–4615. doi:10.1002/mp.14375 [PubMed: 32632928]

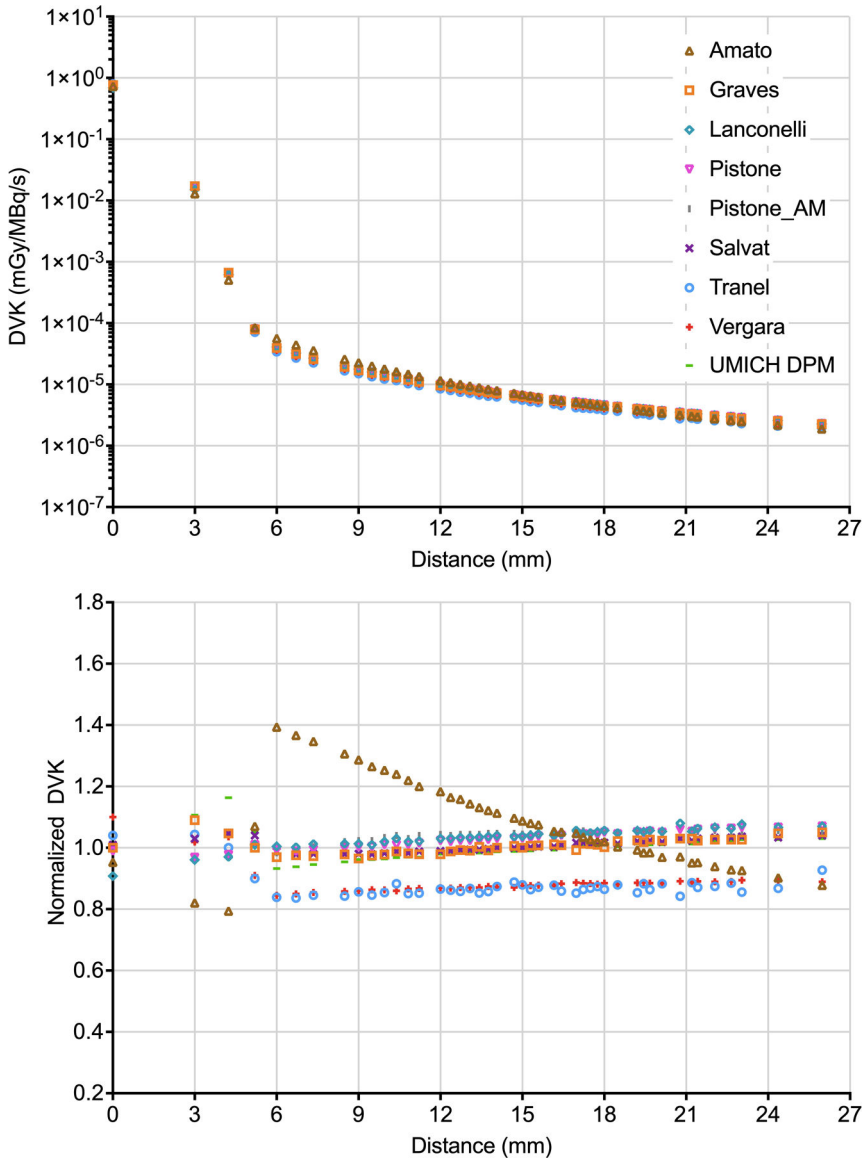

Figure 1:

Top panel - ^{177}Lu DVKs as a function of the distance from the source voxel. *Bottom panel* - normalized ^{177}Lu DVKs as a function of the distance from the source voxel. For better visualization, the values at different voxels but corresponding to the same distance have been averaged.

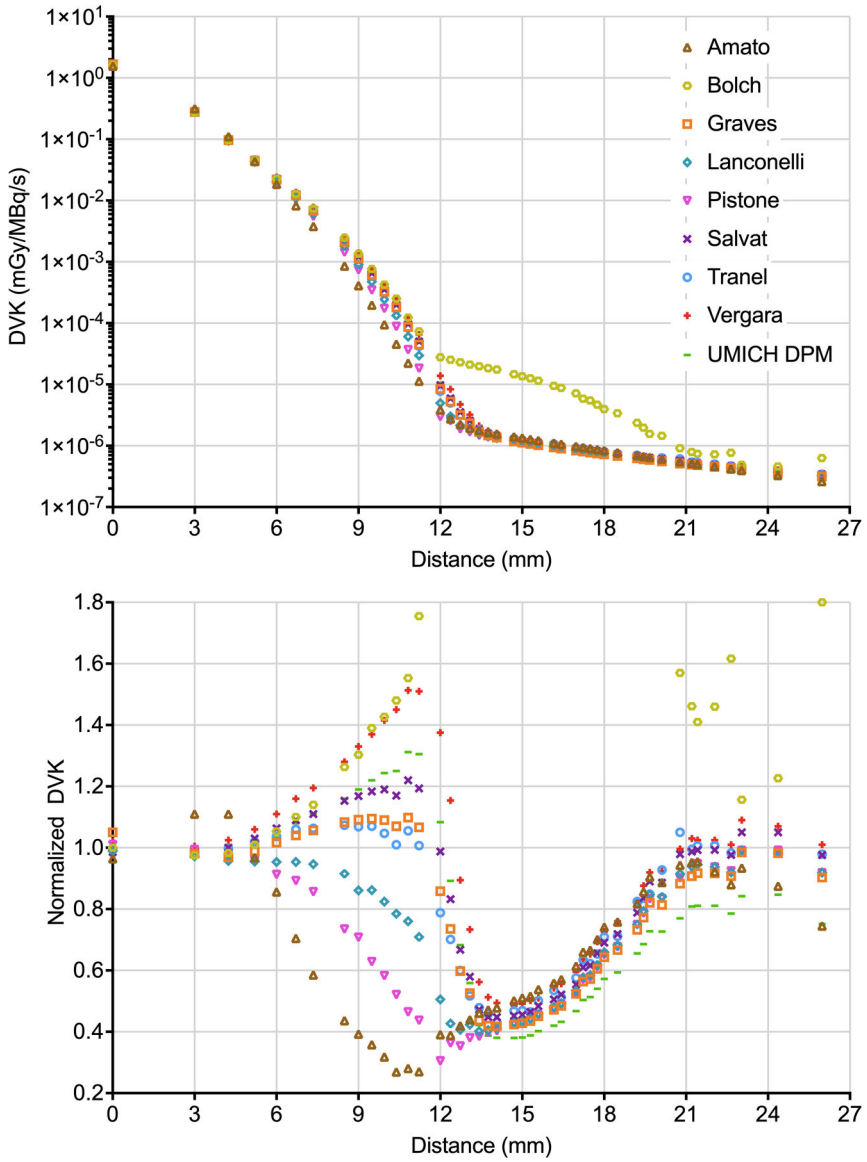

Figure 2:

Top panel - ^{90}Y DVKs as a function of the distance from the source voxel. *Bottom panel* - normalized ^{90}Y DVKs as a function of the distance from the source voxel (part of data from Bolch are out of range). For better visualization, the values at different voxels but corresponding to the same distance have been averaged.

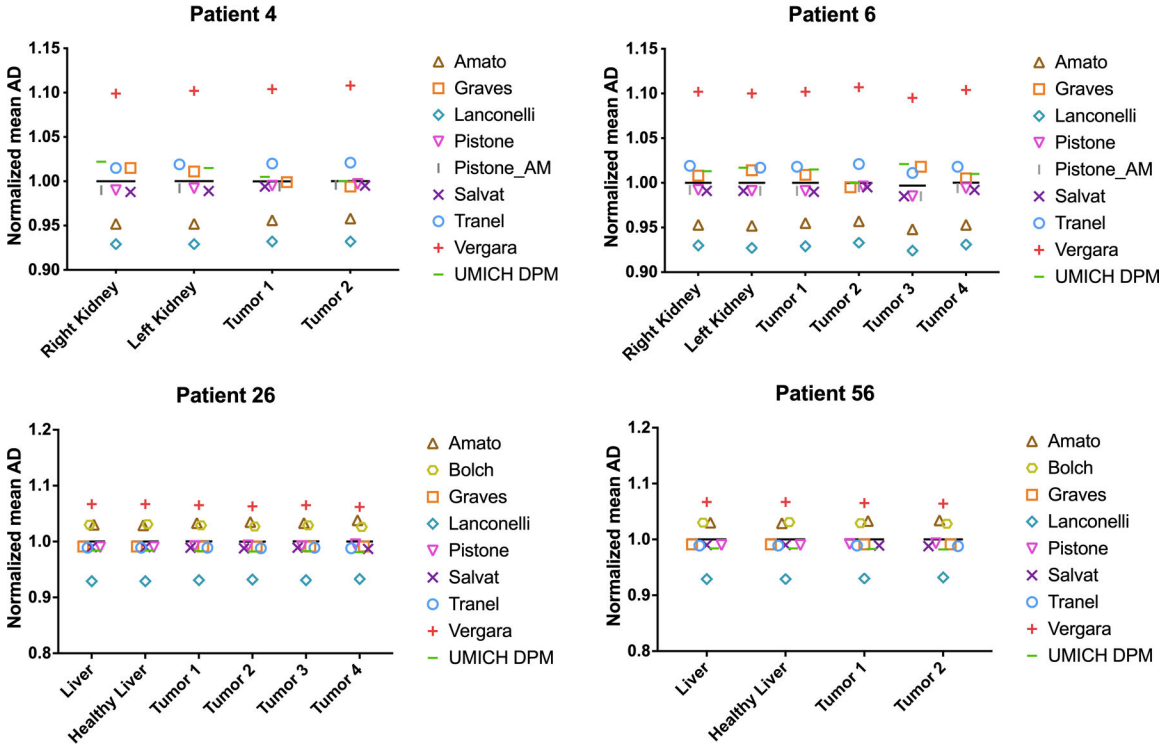

Figure 3:
Mean AD from each kernel divided by the average value from all ADs

Table 1:

Details about the computation methods and setting adopted for all the ^{177}Lu DVKs employed in the present study.

^{177}Lu DVKs	Matrix size	Material composition	Material density	Decay data	Beta spectrum	Calculation method	MC code for DVK or DPK generation	Number of simulated particles	Energy/range cutoff	Surrounding medium
Amato [10]	11×11×11	Soft tissue	1.04 g/cm3	Radar[17]	Radar [*17]	Analytical method	Geant4 9.1	10^8	10 μm	Infinite volume
Graves [8]	275×275×275	Water	1.00 g/cm3	NNDC[18]	Radar[17]	MC volume integration of DPKs	MCNP 6.2	10^6 per emission type	1 keV	Sphere of 2 m radius for DPK
Lanconelli [6]	11×11×11	Soft tissue	1.04 g/cm3	Radar[17]§	Radar [**17]	Direct MC simulation	DOSXYZnrc (EGSnrc)	2.5 *10^7	1 keV	Cubical region with side 16.5 cm
Pistone [7]	15×15×15	Soft tissue	1.03 g/cm3	Radar[17]	Radar[17]	Direct MC simulation	GAMOS 6.2.0	10^9	100 μm	Cubical region with side 50 cm
Pistone_AM [7]	15×15×15	Soft tissue	1.03 g/cm3	Radar[17]	Radar[17]	Analytical method	GAMOS 6.2.0	10^9	100 μm	Cubical region with side 50 cm
Salvat†	11×11×11	Soft tissue	1.00 g/cm3	Nucleide[19]	García-Toraño et al.[20]	Direct MC simulation	PENELOPE (version 2018)[21]	3 *10^8	5 keV (electrons), 1 keV (photons)	Sphere of 20 cm radius
Tranel†	15×15×15	Water	1.00 g/cm3	ENSDF[22]	ENSDF[22]	Direct MC simulation	GATE 9.0	10^8	10 μm	Cubical region with side 1 m
Vergara [9]	11×11×11	Soft tissue≠	1.04 g/cm3	ENSDF[22]	ENSDF[22]	MC volume integration of DPKs	GATE (version not specified)	10^8	1 μm	Cubical region with side 2.1 m
UMICH DPM†	267×267×267	Soft tissue	1.00 g/cm3	NuDat 3.0[23]	BetaShape[24]	Direct MC simulation	Dose Planning Method (DPM)[25]	10^8 (electrons), 4 *10^10 (photons)	20 keV (electrons), 4 keV (photons)	Cubical region with side 267×3mm

†Published within this paper

≠DVK computed by MC volume integration of DPKs in water, converted into soft tissue DVK by the Cross approximation[26].

*merge of monoenergetic e- DVKs, binning: 25 keV

**merge of monoenergetic e- DVKs, binning: 10 keV

§Characteristic x-rays and mono-energetic excluded

Table2:

Details about the computation methods and setting adopted for all the ^{90}Y DVKs employed in the present study.

^{90}Y DVKs	Matrix size	Material composition	Material density	Decay data	Beta spectrum	Calculation method	MC code for DVK or DPK generation	Number of simulated particles	Energy/range cutoff	Surrounding medium
Amato [10]	11×11×11	Soft tissue	1.04 g/cm3	Radar[17]	Radar *[17]	Analytical method	Geant4 9.1	10^8	10 μm	Infinite volume
Bolch [11]	11×11×11	Soft tissue	1.04 g/cm3	Eckerman et al.[27,28]	Not available	Direct MC simulation	EGS4	Not available	Not available	Cubical region with side 24.3 cm
Graves [8]	13×13×13	Water	1.00 g/cm3	NNDC[18]	Radar[17]	MC volume integration of DPKs	MCNP 6.2	10^6 per emission type	1 keV	Sphere of 2 m radius for DPK
Lanconelli [6]	11×11×11	Soft tissue	1.04 g/cm3	Radar[17]§	Radar **[17]	Direct MC simulation	DOSXYZnrc (EGSnrc)	2.5 *10^7	1 keV	Cubical region with side 16.5 cm
Pistone†	15×15×15	Soft tissue	1.03 g/cm3	ENSDF [22]	ENSDF [22]	Direct MC simulation	GAMOS 6.2.0	10^9	100 μm	Cubical region with side 50 cm
Salvat†	11×11×11	Soft tissue	1.00 g/cm3	Nucleide[19]	García-Toraño et al.[20]	Direct MC simulation	PENELOPE (version 2018)[21]	2 *10^8	5 keV (electrons), 1 keV (photons)	Sphere of 20 cm radius
Tranel†	15×15×15	Water	1.00 g/cm3	ENSDF[22]	ENSDF[22]	Direct MC simulation	GATE 9.0	10^8	10 μm	Cubical region with side 1 m
Vergara [9]	11×11×11	Soft tissue‡	1.04 g/cm3	ENSDF[22]	ENSDF[22]	MC volume integration of DPKs	GATE (version not specified)	10^8	1 μm	Cubical region with side 2.1 m
UMICH DPM†	17×17×17	Soft tissue	1.00 g/cm3	NuDat 3.0[23]	BetaShape[24]	Direct MC simulation	DPM[25]	10^9	20 keV (electrons), 4 keV (photons)	Cubical region with side 17×3mm

†Published within this paper

‡DVK computed by MC volume integration of DPKs in water, converted into soft tissue DVK by the Cross approximation[26].

*merge of monoenergetic e- DVKs, binning: 25 keV

**merge of monoenergetic e- DVKs, binning: 10 keV

§Characteristic x-rays and mono-energetic excluded

Med Phys. Author manuscript; available in PMC 2025 January 01.

Table 3:

Average, CoV and % maximum difference of mean AD, D10 and D90 to OARs and tumors in patients treated with a) ^{177}Lu and b) ^{90}Y.

a)	^{177}Lu DOTATATE : Patient 4				^{177}Lu DOTATATE : Patient 6					
	Right Kidney	Left Kidney	Tumor 1	Tumor 2	Right Kidney	Left Kidney	Tumor 1	Tumor 2	Tumor 3	Tumor 4
Mean AD										
Average (Gy)	2.63	2.71	19.80	28.50	5.39	3.43	3.19	30.89	3.09	3.73
CoV	5%	5%	5%	5%	5%	5%	5%	5%	5%	5%
% maximum difference	18%	19%	18%	19%	18%	19%	19%	19%	18%	19%
D10										
Average (Gy)	3.58	3.66	32.74	41.43	7.58	5.19	4.09	39.08	4.39	6.56
CoV	5%	5%	5%	5%	5%	5%	5%	5%	5%	5%
% maximum difference	18%	18%	19%	19%	19%	19%	19%	19%	18%	19%
D90										
Average (Gy)	1.56	1.64	7.84	13.93	2.78	1.79	2.28	21.96	1.70	1.28
CoV	5%	5%	5%	5%	5%	5%	5%	5%	5%	5%
% maximum difference	18%	18%	18%	19%	19%	18%	19%	19%	18%	18%
b)	^{90}Y microspheres: Patient 26						^{90}Y microspheres: Patient 56			
	Liver	Healthy liver	Tumor 1	Tumor 2	Tumor 3	Tumor 4	Liver	Healthy liver	Tumor 1	Tumor 2
Mean AD										
Average (Gy)	67.57	64.68	220.04	450.38	63.52	673.57	52.59	48.39	432.42	107.22
CoV	4%	4%	4%	4%	4%	4%	4%	4%	4%	4%
% maximum difference	15%	15%	14%	14%	14%	14%	15%	15%	14%	14%
D10										
Average (Gy)	180.16	172.58	328.39	727.69	122.25	1051.03	118.56	114.67	681.62	161.56
CoV	4%	4%	4%	4%	4%	4%	4%	4%	4%	4%
% maximum difference	15%	15%	14%	14%	13%	14%	15%	15%	14%	13%
D90										
Average (Gy)	0.46	0.44	119.44	176.70	13.83	293.86	0.32	0.32	230.99	40.64
CoV	4%	4%	4%	4%	4%	4%	4%	4%	4%	4%

a)	^{177}Lu DOTATATE : Patient 4				^{177}Lu DOTATATE : Patient 6					
	Right Kidney	**Left Kidney**	**Tumor 1**	**Tumor 2**	**Right Kidney**	**Left Kidney**	**Tumor 1**	**Tumor 2**	**Tumor 3**	**Tumor 4**
% maximum difference	14%	15%	15%	17%	17%	16%	16%	16%	16%	17%